Olvera-Mancilla, J.; Escorihuela, J.; Alexandrova, L.; Andrio, A.; Garcia-Bernabe, A.; Del Castillo, LF.; Compañ Moreno, V. (2020). Effect of metallacarborane salt H[COSANE] doping on the performance properties of polybenzimidazole membranes for high temperature PEMFCs. Soft Matter. 16(32):7624-7635. https://doi.org/10.1039/d0sm00743a

ARTICLE

Study on cobalt metallacarborane salt H[COSANE] on different polybenzimidazole membranes for high temperature PEMFC applications

Received 00th January 20xx,
Accepted 00th January 20xx

DOI: 10.1039/x0xx00000x

Jessica Olvera,[a] Jorge Escorihuela, *[b], Larissa Alexandrova,[a] Andreu Andrio,[c] Abel García-Bernabé,[d] Luis Felipe del Castillo [a] and Vicente Compañ, *[d]

In this paper, a serie of composite proton exchange membrane comprising a cobaltacarborane protonated $H[Co(C_2B_9H_{11})_2]$ named (H[COSANE]) and polybenzimidazole (PBI) for high temperature proton exchange membrane fuel cell (PEMFC) is reported with the intention of enhancing the proton conductivity of PBI membranes doped with phosphoric acid. The effects of the anion $[Co(C_2B_9H_{11})_2]$ concentration into three different polymeric matrices based on the PBI structure, poly(2,2'–(m–phenylene)–5,5'–bibenzimidazole) (PBI–1), poly [2,2'-(p-oxydiphenylene)-5,5'-bibenzimidazole] (PBI–2) and poly(2,2'–(p–hexafluoroisopropylidene)–5,5'–bibenzimidazole) (PBI–3), have been investigated. The conductivity, diffusivity and mobility is greater in the composite membrane poly(2,2'–(p–hexafluoroisopropylidene)–5,5'–bibenzimidazole) containing fluorinated groups, reaching a maximum when the amount of H[COSANE] was 15%. In general, all the prepared membranes displayed excellent and tunable properties as conducting materials, with conductivities higher than 0.03 $S{\cdot}cm^{-1}$ above 140 °C. From the analysis of electrode polarization (EP) the proton diffusion coefficients and the mobility have been calculated.

Introduction

The increasing CO_2 concentration in Earth's atmosphere from burning of fossil fuels by human activity is a global concern and atmospheric carbon dioxide has reached unprecedented maximum levels above of 400 parts per million (ppm) in the last months.[1] This worrying panorama has conducted industry and academy towards the development on more sustainable energy systems in order to replace traditional combustion technologies. In this outlook, fuel cell technology has emerged as a promising and alternative system of energy transformation.[2,3] Proton conductivity of a polymer electrolyte membrane is one of the critical factors which directly influences the fuel cell performance.[4] To reach high power density in fuel cell technology, the polymeric membrane should possess high proton conductivity, but other parameters such as high chemical, thermal and mechanical stability are also required. In this regard, researchers have devoted efforts to synthetize membranes with high performance to replace the existing Nafion membrane,[5,6] which suffers from elevated cost and low proton conductivity at temperatures over 80 °C, when low hydration conditions are reached. Among the wide variety of alternative polymeric materials which have emerged as proton exchange membranes (PEMs),[7,8] polybenzimidazole (PBI) has emerged in the past decades as an attractive candidate to operate at elevated temperatures. Despite its superior chemical, thermal and mechanical stability when compared with Nafion membranes, proton conductivity in pristine PBI membranes is very low and requires the use of a filler or/and acid doping to reach high conductivity values comparable to those for Nafion-based membranes.[9] To overcome this drawback and enhance the proton conductivity performance of PBI membranes, the use of fillers such as silica,[10,11] metal organic frameworks (MOFs),[12,13] ionic liquids,[14,15] and more recently, metallacarborane and metal oxides,[16] has been widely extended in the fabrication of the so-called mixed matrix membranes (MMMs). The use of this composite materials, which combine an organic polymeric matrix with an inorganic filler, has experienced a blossoming in the last decade.[17,18]

For the design and evaluation of mixed matrix membranes as proton exchange membrane, both components need to be considered. The first constituent of the PEM is the organic matrix, which is known as the continuous phase and along the past decades, a wide family of polymers have been used in the preparation PEMFCs.[19] As mentioned above, PBI (poly(2,2'–(m–phenylene)–5,5'–bibenzimidazole), is an organic heterocyclic polymer with the molecular formula $(C_{20}H_{12}N_4)_n$), which possesses high thermal stability and has been used for high temperature proton exchange membrane fuel cells (HT–PEMFCs).[20,21] Although conductivities up to 0.2 $S{\cdot}cm^{-1}$ can be reached at high acid doping levels, the main drawback of PBI is

[a] Departamento de polímeros, Instituto de Investigaciones en Materiales, Universidad Nacional Autónoma de México (UNAM), Ciudad Universitaria, Apartado Postal 70-360, Coyoacán, Ciudad de México, 04510, México.
[b] Departamento de Química Orgánica, Universitat de València, Av. Vicente Andrés Estellés s/n, Burjassot 46100 Valencia, Spain.
[c] Departament de Física aplicada, Universitat Jaume I, 12080, Castelló, Spain.
[d] Departamento de Termodinámica Aplicada (ETSII), Universitat Politècnica de Valencia, Campus de Vera s/n. 46022 Valencia, Spain.
† Footnotes relating to the title and/or authors should appear here.
Electronic Supplementary Information (ESI) available: [details of any supplementary information available should be included here]. See DOI: 10.1039/x0xx00000x

its weakness upon phosphoric acid (PA) doping which hampers it use as proton exchange membranes. Therefore, in the past decades considerable research has been focused towards the development of alternative PBI polymers to satisfy the desired requirements for fuel cell applications.[22] For this purpose, a few approaches have been developed. One alternative is to add flexible groups, such as ethers, to the polymeric backbone.[23,24] Another approach is based in the introduction of fluorine or fluorine–containing group (i.e. trifluoromethyl group or –CF3) into the polymer structure.[25,26]

The second component of the composite membranes is the inorganic or inorganic-organic filler, which is generally in the form of micro- or nanoparticles and constitutes the dispersed phase. In this regard, our filler is based on cobalt metallacarborane materials, which are inorganic compounds based on polyhedral borane chemistry and transition metal organometallics.[27,28] Metallacarboranes, also named $[Co(C_2B_9H_{11})_2]^-$, are anionic sandwich compounds with a very low charge density, reversible redox electroactive, high stability and great possibilities due to wide range of Eo values (ranging from -1.80 to 0.35 V).[29–31]

In a previous study, we already investigated the temperature dependence of the protonic conductivity of H[COSANE] under wet and dry conditions. From this study, we concluded that conductivity is strongly humidity dependent and was higher in case that H[COSANE] in comparison with other metallacarboranes such as Na[COSANE] and Li[COSANE]. The conductivity of H[COSANE] was similar to other PBI membranes containing carboxylic groups and inorganic fillers, reaching values up to 0.01 $S{\cdot}cm^{-1}$.[32] The hygroscopicity associated to the retention of water has an important influence on the conductivity in salts of $[COSANE]^-$ and the mobility of the protons will be associated to the hydronium ion mobility. On the other hand, the hydridic character of H^+ cation in $[Co(C_2B_9H_{11})_2]^-$ produces that the negative charge is spread on the periphery of the molecule and the mechanism of the transport is basically associate to a Grotthuss mechanism.

In this work, the synthesis and preparation of three different polymeric matrices based on the PBI structure were assayed (Fig. 1), i.e. poly(2,2'–(m–phenylene)–5,5'–bibenzimidazole) (PBI–1), poly [2,2'-(p-oxydiphenylene)-5,5'-bibenzimidazole] (PBI–2) and poly(2,2'–(p–hexafluoroisopropylidene)–5,5'–bibenzimidazole) (PBI–3). Using these three different PBI, different membranes doped with different amounts of the metallacarborane salt H[COSANE] have been prepared and the effect of the filler loading has been evaluated. All composite membranes containing H[COSANE] displayed excellent and tunable properties as conducting materials, reaching conductivities up to 0.031 $S{\cdot}cm^{-1}$. From the analysis of electrode polarization (EP), the proton diffusion coefficients and the mobility have also been calculated.

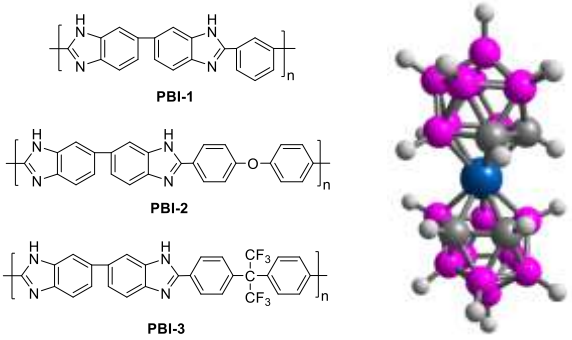

Fig. 1 Chemical structure of PBI polymers used in this study and ball and stick view of H[COSANE].

Results and discussion

Synthesis of PBI polymers.

In our continuous work of developing polymeric membranes based on PBI for PEMFC applications at high temperatures, we decided to evaluate the effect of the PBI structure focused on the conductivity. For this purpose, we used commercial poly(2,2'–(m–phenylene)–5,5'–bibenzimidazole) (named as PBI–1), and two synthesized PBI polymers bearing different groups (Fig. 2): poly [2,2'-(p-oxydiphenylene)-5,5'-bibenzimidazole] (PBI–2) and poly(2,2'–(p–hexafluoroisopropylidene)–5,5'–bibenzimidazole) (PBI–3). All the PBIs present high molecular weight, this property is important in order to prepare good films with excellent mechanical and thermal stability. The polymers used in this study had a molecular weight of 51, 60 and 72 kDa, for PBI–1, PBI–2 and PBI–3, respectively. The synthetic route for both PBI–2 and PBI–3 is based on a polycondensation reaction of 3,3'-diaminobenzidine and the corresponding diacid using Eaton's reagent as both solvent and condensing agent.[33] In this regard, PBI–2 and PBI–3 were prepared by mixing a w/w% ratio [monomer] : [ER] of 7 : 93 at 180 °C in 7 and 20 min respectively.

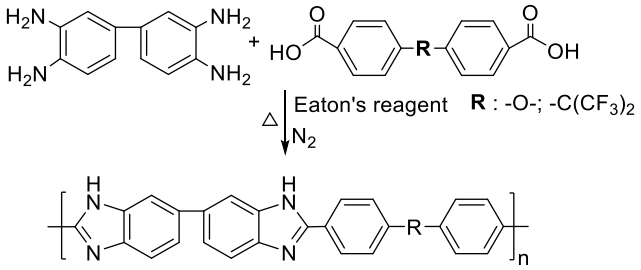

Fig. 2 Synthesis route for polybenzimidazoles.

After PBI isolation and drying, the synthesized polymers were characterized by nuclear magnetic resonance spectroscopy (NMR). The ^1H NMR spectra (measured in deuterated dimethyl sulfoxide ($DMSO\text{-}d_6$)) shown in Fig. 3 confirmed the polymer structures and showed that the solvent had been effectively eliminated, with integral values in accordance with the expected chemical structures. In the case of PBI–2, the peak attributed to the imidazole proton was observed at 13.01 ppm, and aromatic protons were at 7.0–8.5 ppm (Fig. 3A). For PBI–3, the imidazole proton peak shifted, as expected to the electronic effects, to 13.20 ppm (Fig. 3B).

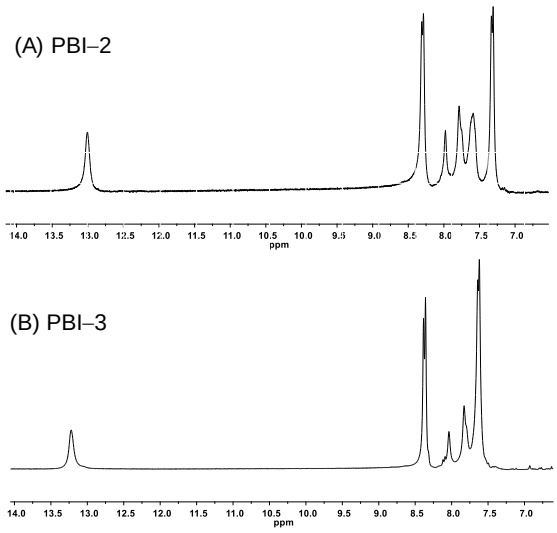

Fig. 3 ^{1}H NMR spectra in DMSO-d_6 of (A) PBI–2 and (B) PBI–3.

All PBIs were characterized by means of Fourier transform infrared spectroscopy (FTIR) and the corresponding spectra are shown in Fig. 4. IR spectrum of commercial PBI–1 displayed a broad band around 3600–3100 cm^{-1}, corresponding to the N–H stretching, and peaks at 1605 and 1425 cm^{-1}, attributed to C=N and C–N stretching vibrations, respectively.[34] Additionally, the absorption peak attributed to the stretching of the imidazolate ring (C–C) was also observed at 1455 cm^{-1}.[35] For PBI–2, a broad band corresponding to C=N and C=C bonds vibrations of benzimidazole skeleton was observed at 1630–1600 cm^{-1}. The peaks at 1580 and 1420 cm^{-1} were associated to different vibrations of the benzene ring, and the band centerd at 1175 cm^{-1} was referred to the Ar–O–Ar vibration.[36] Finally, PBI–3 exhibited all characteristic absorption bands previously described for this polymer.[37,38] The N–H stretching vibrations of the benzimidazole ring were observed in the range of 3500–2800 cm^{-1}, the bands at 1630 cm^{-1} and 1550–1400 cm^{-1} were assigned to C=N and C=C vibrations, respectively; additional absorptions between 1260 and 1115 cm^{-1} corresponding to the C–F stretching vibrations were observed.[39,40]

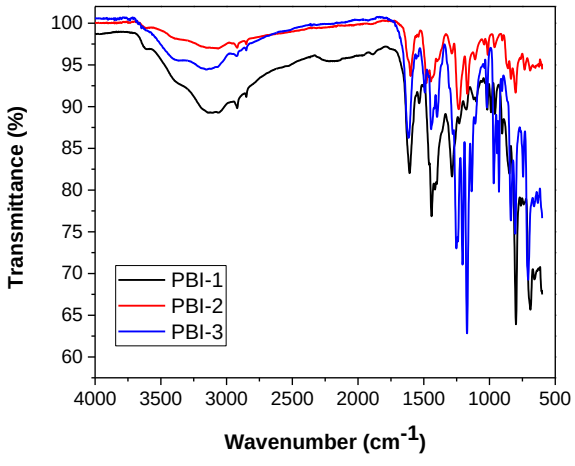

Fig. 4 FTIR of PBI–1 (black line), PBI–2 (red line) and PBI–3 (blue line).

The TGA analysis performed under a nitrogen atmosphere for the two prepared PBIs, i.e. PBI–2 and PBI–3, are displayed in Fig. 5. Both synthesized polymers had elevated thermal stability; the principal weight loss for both samples was observed at temperatures above 520 °C. The PBI–2 sample showed a weight loss around 5–7% at 140 °C, due to desorption of water molecules. A small weight loss, was noticed at temperatures higher than 300 °C, which is frequently observed in OPBIs and is attributed to the evaporation of the coordinated water.[41]

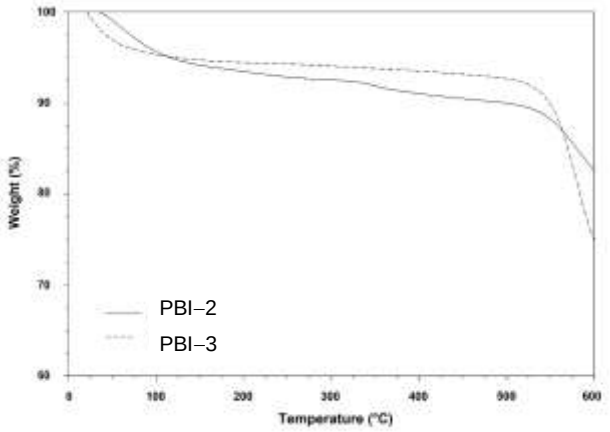

Fig. 5 TGA curves of PBI–2 and PBI–3 under a nitrogen atmosphere.

Preparation and characterization of PBI composite membranes.

Next, composite membranes containing H[COSANE] were prepared by traditional casting method (Fig. 6). For that, one gram of the corresponding polybenzimidazole (PBI–1, PBI–2 or PBI–3) was dissolved in 10 mL of dimethyl acetamide (DMAc) to prepare a 10 wt% solution of PBI. Next, varying amounts of 10, 15, 20 and 30 mg of H[COSANE] were added for the required weight percentage (10, 15, 20 and 30 wt%, respectively), dispersed in the PBI solution and sonicated for 1 h followed by continuous stirring for 24 h. The resultant solution was individually cast on a flat glass plate and dried at 80 °C for 8 h, and at 140 °C for 24 h to remove the residual DMAc solvent. The dried membrane was then peeled off from the plate and finally dried under vacuum at 160 °C for 30 min. The average thickness of the membranes was around 70 mm. These membranes were labeled as PBI–1@A% H[COSANE], PBI–2@A% H[COSANE], and PBI–3@A% H[COSANE], where A is the loading of H[COSANE] (A = 10, 15, 20 and 30 wt%). After addition of the H[COSANE] filler to the polymeric matrix, an additional band appeared in the FTIR spectra of all composite membranes at 2540 cm^{-1} attributed to the B–H stretching vibrations of H[COSANE].

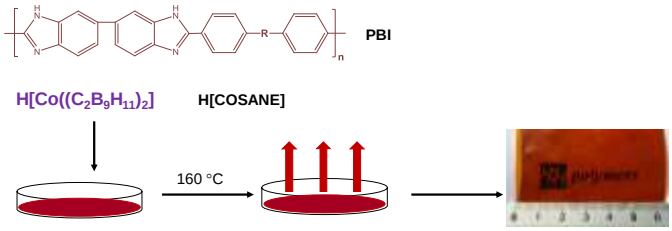

Fig. 6 Schematic representation of membrane preparation by the casting method.

The internal microscopic morphologies of different PBI membranes were analyzed by field emission scanning electron microscope (FE–SEM). The cryofractured cross sections of the different PBI membranes are shown in Fig. 7. The cryofractured surface of the PBI membranes was dense and homogeneous, without holes. However, the addition of H[COSANE] as filler produced the appearance of holes in the cryofractured cross sections, as shown in the FE–SEM images. After doping the membranes with PA, the morphology of all membranes showed the formation of channels, which are generally attributed to the presence of PA in the polymer, as observed in other PBI membranes.[42]

To assure an adequate proton transport and use our composite membranes as PEM in a fuel cell configuration at moderate or high temperatures, it is necessary that the polymer electrolyte membrane displays high thermal stability at elevated temperatures being a required parameter for a polymer electrolyte membrane in a membrane assembly electrodes (MEA) configuration. For comparison, the undoped membranes were characterized by TGA (see Fig. 8, black lines). The polymeric membranes displayed high thermal stability; the main weight loss was observed at 600 °C for PBI–1 and PBI–2, but at temperature around 530 °C for PBI–3. The PBI–1 thermogram presents a drop at 130 °C with a weight loss of 11% due to desorption of water, and the PBI–2 and PBI–3 samples show weight losses around 5–7% at the same temperature. A weight drop lowered than 10% was noticed at higher temperatures (250–300 °C) frequently noticed in PBIs by evaporation of the coordinated water.[43,44]

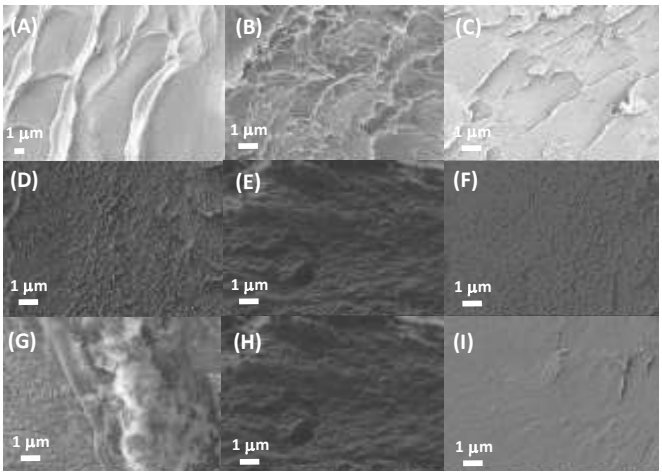

Fig. 7 SEM images of cryofractured PBI membranes: (A) PBI–1; (B) PBI–1@10%H[COSANE]; (C) PBI–1@30%H[COSANE]; (D) PBI–2; (E) PBI–2@10%H[COSANE]; (F) PBI–2@30%H[COSANE]; (G) PBI–3; (H) PBI–3@10%H[COSANE] and (I) PBI–3@30%H[COSANE].

Next, the thermal behavior of PBI-based membranes with different amounts of H[COSANE] (10, 15, 20 and 30 wt%) was analyzed by TGA (Fig. 8). The TGAs obtained under a N_2 atmosphere for PBI–1 in presence of H[COSANE] in the different proportions all the curves present a drop weight around 100 °C, the weight % diminished when the amount of H[COSANE] increased, then the drop around 300 °C for PBI–1 is recorded at low temperature around 250 °C when the H[COSANE] is present. The main weight loss increase from 550 °C without H[COSANE] to 700 °C when the 20 wt% of H[COSANE] is present, at 30 wt% of H[COSANE] the temperature of decomposition is in 650 °C, however this higher than PBI–1 pristine. The PBI–2 present a similar behavior than with PBI–1 with the presence of H[COSANE], at 100 °C the weight % diminished when the PBI–2@H[COSANE] increase. Then in general a second drop is present around 220 °C in presence of H[COSANE], the main loss weight of the polymers appears between 500–650 °C, the temperature increase with the increase of ratio PBI–2@H[COSANE]. In contrast, the curves by PBI–3 remain similar in absence and presence of H[COSANE], the main weight loss is around 520 °C for all samples.

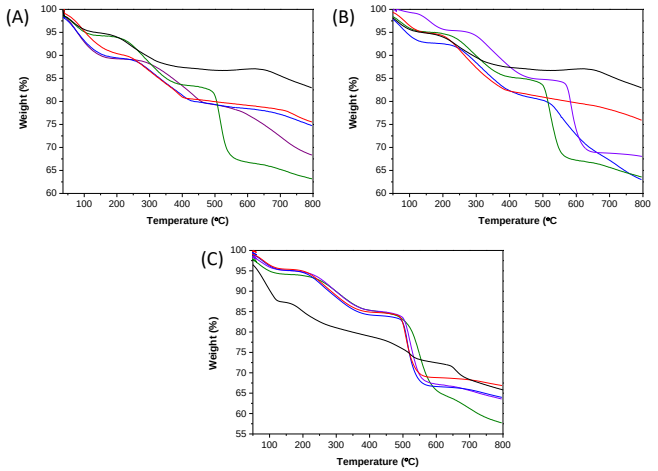

Fig. 8 Thermal stability of different composite membranes containing H[COSANE] at different concentrations 0 (——), 10 (——), 15 (——), 20 (——) and 30 (——) wt %) for (A) PBI–1, (B) PBI–2 and (C) PBI–3.

PBI membranes can be doped by immersion in an aqueous phosphoric acid solution (1 M) at room temperature. Higher doping levels increase the membrane conductivity; however, the mechanical strength is weakened. Therefore, a commitment must be taken between these two properties. Generally, after 48 hours the equilibrium is reached and membranes with a doping level of 5–6 mol phosphoric acid per repeating unit of PBI. Acid uptake (AU) after immersion in 1 M H_3PO_4 aqueous solution, acid uptake values were

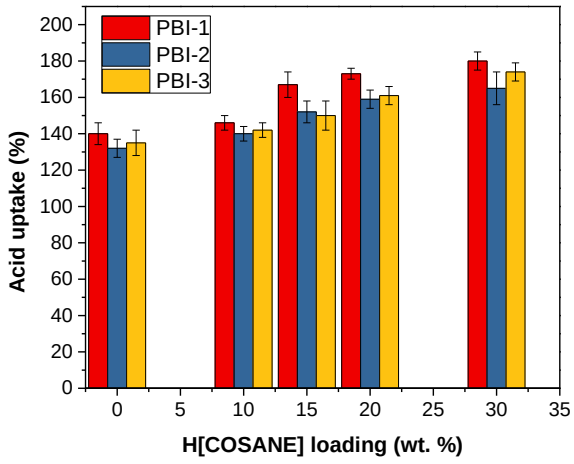

Fig. 9 Acid uptake of composite membranes containing H[COSANE] at different concentrations (0, 10, 15, 20 and 30 wt %) for PBI–1, PBI–2 and PBI–3.

calculated from weight difference and in general, acid uptake around 150% were obtained (Fig. 9). The prepared polymeric membranes were stable, and no coloration was observed even after 2-day immersion in 1 M H_3PO_4.

The oxidative stability of the composite membranes is a critical parameter for its future applicability as PEMFC, as radicals (•OOH and •OH) are generated during the fuel cell operation can cause the degradation of the membrane by a radical oxidation process. To this end, the oxidative stability was evaluated by Fenton's test.[45] In this study, the composite membranes were immersed in 3% H_2O_2 aqueous solution containing 3 ppm Fe^{2+} at 80 °C and the weight loss at different times was recorded as indicated in Table 1. When compared with the pristine PBI membrane (0 wt% of H[COSANE]), the composite membranes exhibited superior stability to radical oxidation. In this regard, resistance to oxidative stability after 24 h increased with the increasing content of H[COSANE] following the trend: PBI-1 < PBI-1@10%COSANE < PBI-1@15%COSANE < PBI-1@20%COSANE < PBI-1@30%COSANE. As observed, membrane with high content of H[COSANE] was not stable in Fenton's solution and broke after 96 h. Similar trends were observed for composite membranes PBI-2 and PBI-3.

Table 1. Oxidative stability measured by weight loss evaluated by Fenton's test for PBI–3 membranes.

	Weight loss (%)		
H[COSANE] wt%	**After 12 h**	**After 24 h**	**After 96 h**
0	13	22	36
10	11	19	26
15	10	17	25
20	10	15	22
30	10	14	Break

Proton conductivity of mixed matrix membranes.

In order to analyze the proton conductivity of the composite membranes, electrochemical impedance spectroscopy measurements were performed on the phosphoric acid based-PBI membranes with different loadings of H[COSANE] in the polymeric matrix. In order to get information about the proton transport, electrochemical impedance spectroscopy (EIS) was used to measure the proton conductivity of the composite membranes.[46,47] The measurements were carried out at different temperatures at frequencies varying from 0.1 Hz to 10 MHz, between 20 and 200 °C with steps of 20 °C. The values of the proton conductivity were calculated from corresponding Bode diagrams. Initially, conductivity measurements were performed on undoped PBI–1@10%HCOSANE membrane (**Fig. S1**). From these measurements, very low conductivity (~10^{-8} S·cm^{-1}.) was observed for the composite membrane along the range of temperatures under study. This phenomena can be rationalized by a Debye relaxation associated to the motion and reorientation of the dipoles and localized charges as consequence of the applied electric field, which dominates the dc-conductivity.[48–51]

In order to improve their performance, membranes were doped by immersion on a 1 M phosphoric acid solution for 2 days, when saturation conditions were reached. Fig. 10 shows the variation of

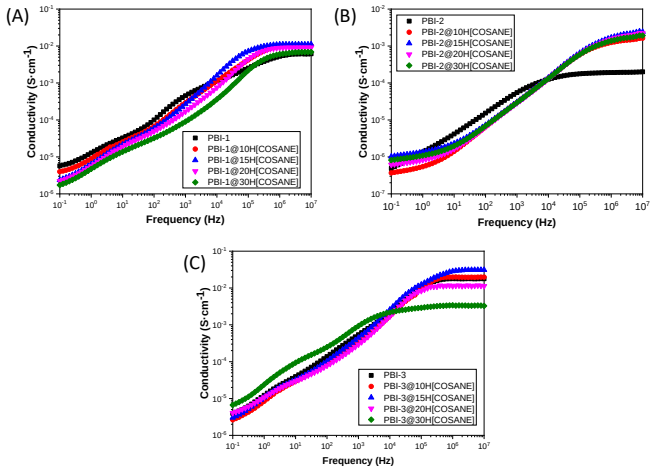

Fig. 10 Double logarithmic plot of the real part of the conductivity versus frequency for PBI–1, PBI–2, and PBI–3 at 140 °C and different amount of A%H[COSANE] (A = 0, 10, 15, 20, 30 wt%).

the proton conductivity with the frequency for all composite membranes at 140 °C. From this figure, it can be observed that proton conductivity is dependent on the amount of H[COSANE] incorporated in the polymeric matrix of PBI and also on the structure of PBI. In all the composite membranes, conductivity increased with the loading of H[COSANE], until a concentration of 15 wt%; however, the conductivity decreased from this value, which can be caused by the agglomeration of H[COSANE] in the polymeric matrix. On the other hand, the values in conductivity are higher in case of PBI–3 and PBI–1, indicating that the interaction of the charge with the polymer matrix is more suitable in PBI–1 and PBI–3 than for PBI–2. For all temperatures under study, the conductivity of composite membranes increased with temperature, following the trend, σ' (PBI–3) > σ' (PBI–1) > σ' (PBI–2).

In the case of measurements under wet conditions (from 20 to 80 ºC), a deviation from σ_{dc} in the spectrum of the conductivity at low frequencies was observed (see Fig. S2–S11), which might be attributed to the electrode polarization (EP) effect as consequence of the blocking electrodes, and produced by the accumulation of mobile charges. When comparing regions of high and low frequencies, a decrease in conductivity was observed, associated to a Debye relaxation, whose time relaxation depends on the chemical structure of the polymer, membrane thickness and measurements conditions, such as temperature and humidity.[52–54]

Fig. 11 displays the Bode plot for all the composite membranes with 15 wt% of H[COSANE] at 100–200 °C. From this figure, which shows the conductivity (in S·cm^{-1}) vs. frequency in (Hz) of each sample in the interval of temperatures from 100 to 200 °C, we can see a temperature dependence of the conductivity. At low temperatures, σ_{dc} notably depends on the frequency and this effect tends to disappear when the temperature increases. The real part of the conductivity, σ', is characterized in the Bode plot by a plateau, where the phase angle tends to zero. In this situation, the imaginary part of the impedance will be zero, and then the corresponding conductivity represents the direct-current conductivity (σ_{dc}) of the

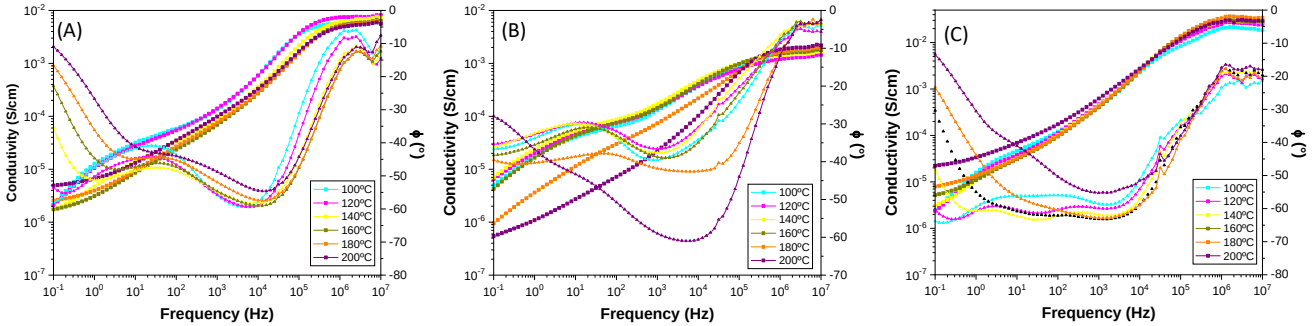

Fig. 11 Bode plots for PBI–1@15%HCOSANE, PBI–2@15%HCOSANE, and PBI–3@15%HCOSANE at different temperatures (100–200 °C).

membrane. The emergence of a plateau associated with the conductivity plots shifts at low temperatures and is not significantly remarkable for all the samples. For example, for the PBI–3@15%COSANE membrane, the conductivity at 180 °C was around 3.1×10^{-2} S·cm^{-1}, being around seven times higher than PBI–1@15%COSANE and 16 times higher than PBI–2@15%COSANE. In all the range of temperatures studied the conductivity increased with temperature following the trends σ′ (PBI–3@H[COSANE],) > σ′ (PBI–1@H[COSANE]) > σ′ (PBI–2@H[COSANE]) > σ′ (PBI), independent of %wt of COSANE.

Table 2. Proton conductivity of PBI membranes doped with different fillers reported in literature.

Filler	σ_{dc} (S·cm^{-1})	Conditions	Reference
5 wt% H[COSANE]	0.031	180 °C	This work
5 wt% ZIF-8/ZIF-67	0.091	200 °C	[13]
5 wt% BMIM-NTf$_2$	0.098	120 °C	[16]
3 wt% RGO	0.028	170 °C	[21]
GO-Fe$_3$O$_4$	0.056	80 °C	[58]
MWCNTs	0.074	180 °C	[59]
5 wt% GO	0.170	180 °C	[60]
30 wt% Ph silane	0.130	180 °C	[61]
10 wt% Si NPs	0.250	200 °C	[62]
15 wt% LAMS	0.181	160 °C	[63]
50 wt% Zr(PBTC)	0.067	200 °C	[64]
Phosphonated CNTs	0.120	140 °C	[65]
2 wt% Sulfonated GO	0.052	175 °C	[66]
DESH	0.040	200 °C	[67]

ZIF: zeolitic imidazole framework; LAMS: s long chain amine modified silica; NPs: nanoparticle; BMIM-NTf$_2$: 1-Butyl-3-methylimidazolium bis(trifluoromethylsulfonyl)imide; MWCNTs: multi-walled carbon nanotubes; GO: graphene oxide; RGO: reduced graphene oxide; Zr(PBTC): zirconium tricarboxybutylphosphonate; DESH: diethlyamine sulphuric acid.

The conductivities obtained in this work are around 30 mS·cm^{-1}, and corresponds to the composite membrane PBI–3@15%H[COSANE at 140 °C. This conductivity is comparable with other membranes based PBI such as the case of hexafluoropropylidene based PBI membranes, with proton conductivity of 49 mS·cm^{-1} measured at 120 °C.[55] Therefore, our results are particularly encouraging. In fact, they are comparable with other reported membranes of *m*–PBI or *p*–PBI with higher doping levels and higher working temperatures (150–200 °C).[56,57] The observed conductivities are in the same order of magnitude than those observed for other PBI membranes doped with other fillers (**Table 2**); however some of the reported values are given on measurements along the plane of the membrane, which generally is reflected in higher values than the through-plane measurements reported here.

The dependence of the conductivity with temperature was studied for all the composite membranes by means of a typical Arrhenius plot, where the ln σ_{dc} is plotted *vs*. 1000/T. From this graphical representation (Fig. 12), we can see that conductivity followed a Arrhenius behavior with two different sections: the first one, located between 20 and 160 °C, where the conductivity of most of the composites increased with temperature, following the Arrhenius equation

$$ln\,\sigma_{dc} = ln\,\sigma_{\infty} - \frac{E_{act}}{RT} \qquad (1)$$

and the second one, for temperatures above 160 °C, where the conductivity strongly began to decrease due to the loss of phosphoric acid.

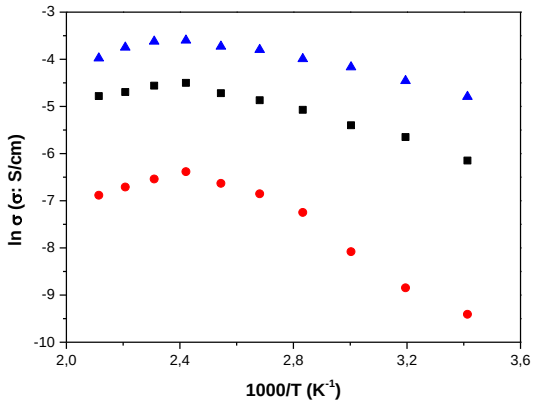

Fig. 12 Conductivity versus reciprocal of temperature for PBI–1@15%H[COSANE],) (■), PBI–2@15%H[COSANE],) (●), and PBI–3@15%H[COSANE],) (▲), respectively.

The activation energy associated to the proton transport were calculated with the slopes of the fits according to Equation 1, and the values are shown in Table 3. The obtained values for the composite

membranes containing 15 wt% of H[COSANE] followed the trend: E_{act}(PBI–3) < E_{act}(PBI–1) < E_{act}(PBI–2). A similar tendency was observed for the others amounts of filling agent H[COSANE]. These results indicate that the optimal doping percentage of H[COSANE] is 15 wt%. As expected, all E_{act} values for the composite membranes were higher than those obtained for the filler itself (E_{act}H[COSANE] = 5.6 kJ·mol^{-1}). The aforementioned results indicate that the proton conduction process is most favorable for PBI–3, which contains two CF_3 groups on its structure and may facilitate the transport through the hydrogen bond network. In general, these values are lower than those found in similar composites such as PEDOT:H[COSANE], whose E_{act} was around 36.4 kJ·mol^{-1},[68] and slightly higher than Nafion membranes, which value are about 10.5 kJ·mol^{-1}.[69] On the other hand, these PBI composites showed activation energies significantly lower than polycristaline salts of CsH_2PO_4 and CsH_2PO_4/silica composites, whose values are around 38.6 and 48.3 kJ·mol^{-1} respectively.[70] This behavior can be associated to the variation in Debye's length, which is related with the effective dissociation energy and the measured dielectric permittivity in absence of electrode polarization (ε_∞), as well as of orientational polarization of dipolar ions, as previously reported.[71,72] The activation energy values for conduction in our composite membranes are smaller than the PBI membranes without H[COSANE] where the values are respectively 16.2, 17.5 and 23.6 kJ·mol^{-1} for PBI–3@H[COSANE], PBI–1@H[COSANE] and PBI–2@H[COSANE], respectively. On the other hand, our results are similar to the values reported for membraned filled with ionic liquids,[16] which values are near 23.3 kJ·mol^{-1} and are comparable to those reported by Rivera and Rossler for other imidazolium based ILs.[73]

Table 3. Activation energy values calculated from Arrhenius plot for the different composite membranes.

	E_{act} (kJ·mol^{-1})		
H[COSANE] wt%	PBI–1	PBI–2 E_{act}	PBI–3
0	17.5 ± 2.2	23.6 ± 2.1	16.2 ± 1.6
10	15.5 ± 1.8	33.5 ± 2.9	17.5 ± 1.5
15	13.3 ± 1.3	26.9 ± 2.6	9.9 ± 1.0
20	12.0 ± 1.2	33.9 ± 2.9	12.4 ± 1.1
30	12.3 ± 1.2	36.0 ± 3.1	14.5 ± 1.4

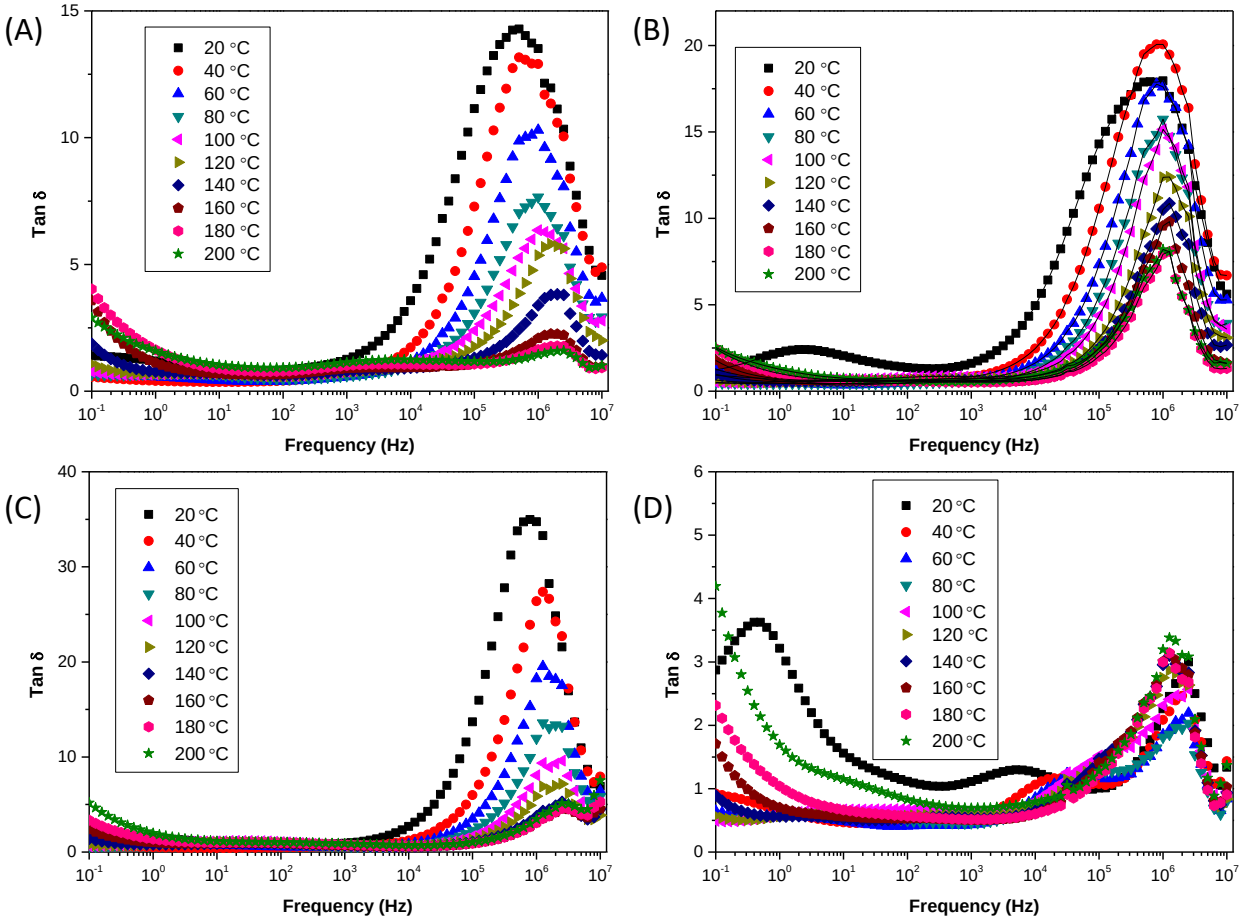

Fig. 13 Temperature dependence of Tan δ for the composite membranes (A) PBI–1@10%H[COSANE], (B) PBI–1@15%H[COSANE], (C) PBI–3@10%H[COSANE] and (D) PBI–3@15%H[COSANE]

.

Two possible mechanisms for the conduction pathway are generally accepted in composite membranes. The Grotthuss mechanism is given by means of the interaction of protons through jumps along a hydrogen bond network of N–H groups present in the PBI chains, and vehicular mechanism by means of the imidazole groups present in the PBI and more concretely from phosphoric groups presents into the cavities of COSANE and PBI matrix. The evaporation temperature of phosphoric acid is around 160 °C and accordingly the conductivity of the membranes decreases above this temperature. Similar results have been found in proton exchange membranes based on semi-interpenetrating polymer networks of polybenzimidazol and perfluorosulfonic acid polymer containing hollow silica spheres as inorganic filler.[74]

Difussivity and mobility.

In binary systems such as salt/polymer solutions, both cations and anions participate in the conduction process, although a large fraction can be bound up in ion pairs or clusters and therefore, the total density of carrier concentration can be difficult to quantify. However, from the analysis of electrode polarization (EP) based on the Trukhan theory, an estimation of the diffusion coefficients (*D*) from the values of tan δ can be made, being d the phase angle of the complex dielectric permittivity. Assuming that anion and cation have equal diffusion coefficients *D*+ and *D*-, the Macdonald-Trukhan model[75–78] allows to derive an explicit expression for the diffusion coefficient (*D*) according to

$$D = \frac{2\pi f_{max}^{\tan\delta} \cdot L^2}{32\,[(tan\ \delta)_{max}]^3} \qquad (2)$$

where, $(tan\ \delta)_{max}$ is the maximum value of ε''/ε' in the frequency range of electrode polarization, $f_{max}^{\tan\delta}$ is the frequency at the $tan\ \delta$ reach a maximum and L the membrane thickness.

Fig. 13 shows the tan d as a function of the frequency, where a clear maximum is observed at the characteristic frequency at which the value of conductivity of the composite membranes has been determined. Notice that the Bode diagram of the conductivity showed a plateau in the range of temperatures where tan δ reached a maximum. Taking the cut-off frequency as the onset of electrode polarization (EP), which can be defined as the maximum in tan d, the diffusion coefficient (*D*) as a function of the temperature can be calculated using Equation 2. When comparing the intensity of the loss tangent in both PBI matrix, PBI–3@10%H[COSANE] and PBI–3@15%H[COSANE], respectively, we can observe that PBI–1 has a higher intensity than PBI–3, when filled with H[COSANE]. This can be attributed to the presence of CF_3 groups on PBI matrix, which may produce a decrease of the intensity. On the other hand, the intensity of the loss tangent decreased with temperature and shifted with temperature to high frequencies. Finally, the inclusion of the H[COSANE] produced wider peaks; meaning that the width frequency changed in one decade.

Fig. 14 displays the diffusion coefficient of protons (*D*) versus temperature for PBI–1@H[COSANE] and PBI–3@H[COSANE] in terms of the Arrhenius plot. A close inspection of these figures showed, in both samples, that diffusivity increased with temperature and with the amount of H[COSANE] until the 15 wt%, after which it decreased. On the other hand, different behavior was observed for PBI–1 and PBI–3. While in the composite PBI–3 the diffusivity increased with temperature until reaching a constant value around 180–200 and C, for PBI–1 the maximum value was reached at 140–160. The activation energy associated to the diffusivity followed the trend E_{act} (PBI–3) < E_{act} (PBI–1) independently of the content of H[COSANE], being lower for the sample PBI–3@15%H[COSANE], whose value was around 11.4 ± 0.7 kJ·mol^{-1}.

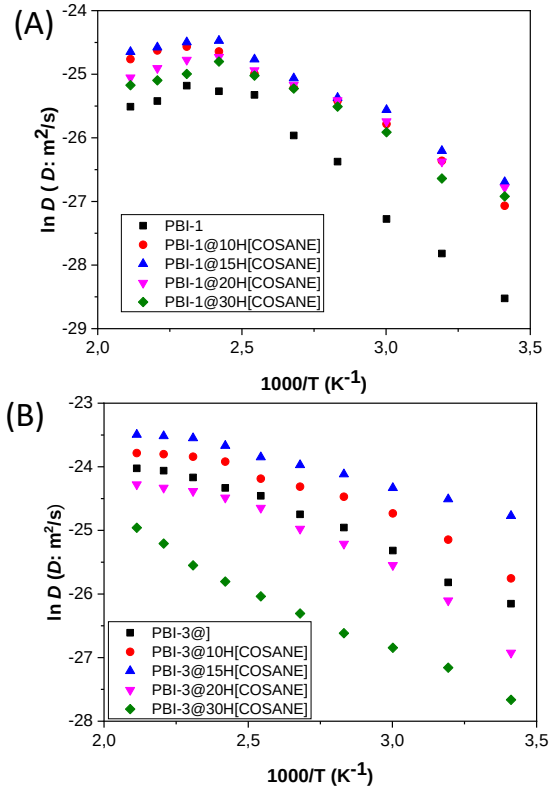

Fig. 14 Temperature dependence of proton diffusivity for composite membrane (A) PBI–1@H[COSANE]. and (B) PBI–3@H[COSANE] both at 0, 10, 15, 20 and 30 wt% of H[COSANE].

Finally, the ion mobility (μ) from the Nernst-Einstein relation can be calculated from the diffusivities (*D*) according to the following expression

$$\mu = \frac{q\ D}{k_B T} \qquad (3)$$

where k_B is the Boltzmann constant and *q* the amount of charge carried by an ion (*q*=|Z| e); (i.e. the proton charge). Fig. 15 displays the proton mobilities calculated from Equation 3 as a function of temperature. The graphical representation showed a similar behavior to the plot of diffusivities, where the sample PBI–3@15%H[COSANE] had the highest conductivity and mobility of the series. On the other hand, these results, as expected, gave diffusivities and mobilities values lower than protons in water, whose value is around 10×10^{-9} $m^2 \cdot V^{-1} \cdot s^{-1}$, as obtained theoretically and experimentally.[79,80]

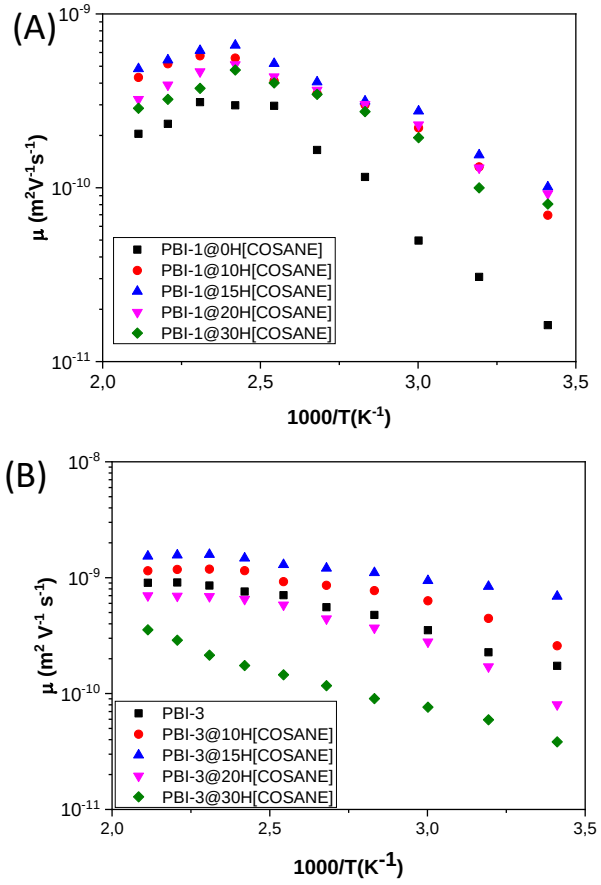

Fig. 15 Variation of the mobility with the inverse of temperature for the composite membranes (A) PBI–1@A%H[COSANE] and (B) PBI–3@A%H[COSANE] both at 0, 10, 15, 20 and 30 wt% of H[COSANE].

Considering that anion and cation have equal diffusion coefficients D^+ and D^-, the diffusivity can be estimated applying the Nernst-Einstein equation

$$D = \frac{\sigma RT}{F^2 C_+} \quad (4)$$

where s is the dc-conductivity, R the gas constant (8.3144 $J{\cdot}K^{-1}{\cdot}mol^{-1}$), T is the absolute temperature, F is the Faraday`s constant, and C_+ is the concentration of ions in the membrane (the value is estimated considering that the phosphoric acid concentration was 0.0193 mol of H^+ in the volume of the synthetized membrane, 15.7×10^{-9} m^3). A comparison at 140 °C, between the proton diffusion coefficient obtained from Equation 3, 5.3×10^{-11} $m^2{\cdot}s^{-1}$, and the stoichiometrically calculated from Equation 4, 1.0×10^{-11} $m^2{\cdot}s^{-1}$, indicates that there is an overestimation of the theoretically calculated values with respect to those determined using stoichiometric values. This result clearly indicates the Trukhan model describes qualitatively the dielectric response but may fail to give quantitative values as a consequence of the difference between the free-proton number density respect the total proton number density at complete dissociation from the electrode polarization analysis.[81]

Conclusions

In summary, we have prepared polymeric composite membranes based on three different PBIs containing cobaltacarborane protonated $H[Co(C_2B_9H_{11})_2]$, named (H[COSANE]) at different loadings and doped with 1 M phosphoric acid. The composite membranes were characterized by ^1H NMR, TGA, FE–SEM and conductivity in the transverse direction by electrochemical impedance spectroscopy (EIS). The effects of the anion [Co(C2B9H11)2] amount into three different polymeric PBI matrices, namely poly(2,2'–(m–phenylene)–5,5'–bibenzimidazole) (PBI–1), poly [2,2'-(p-oxydiphenylene)-5,5'-bibenzimidazole] (PBI–2) and poly(2,2'–(p–hexafluoroisopropylidene)–5,5'–bibenzimidazole) (PBI–3), have been investigated using the electrode polarization (EP) model based on the Trukhan theory. The estimation of the diffusion coefficients and mobility's were calculated from the values of tan δ. The activation energy associated to the conductivity values for the composite membranes containing 15 wt% of H[COSANE] followed the trend E_{act} (PBI–3@H[COSANE])= 9.9 < E_{act} (PBI–1@H[COSANE) = 13.3 < E_{act} (PBI–2@H[COSANE)= 26.9 $kJ{\cdot}mol^{-1}$. A similar tendency has been observed for the others amount of doped agent H[COSANE]. These results indicate that the optimal doping percentage of H[COSANE) was 15 wt%. Similar results have been found in diffusivity and mobility where both parameters reached higher values in the PBI–3 composite membrane. In general, all prepared membranes displayed excellent behaviour as conducting materials, with conductivities higher than 0.03 $S{\cdot}cm^{-1}$ above 140 °C. These values indicate that PBIs containing cobaltacarborane protonated H[COSANE] can be a promising alternative to be used in different energy devices fundamentally making a potential candidate to operate in the range of 120 to 160 °C as HT–PEMFCs. Further applications of these materials are currently under investigation.

Experimental

Materials and methods.

Chemicals. Poly(2,2'–(m–phenylene)–5,5'–bibenzimidazole), also known as *meta*–PBI or simply PBI with molecular formula $(C_{20}H_{12}N_4)_n$), (MW 51 kDa, purity > 99.95%) was purchased from Danish Power Systems. Lithium chloride (LiCl), N,N-dimethylacetamide (DMAc) 99.8%, concentrated phosphoric acid (85% solution in water) were purchased from Scharlab. The monomers 3,3'-diaminobenzidine (TAB, 99%) and 4,4'-oxybis(benzoic acid) (OBBA, 99%) were supplied from Aldrich; the diacid 4,4'-(hexafluoroisopropylidene)bis(benzoic acid) (HFA) was provided by Central Glass Co., Ltd., Japan. The N,N'-Dimethylformamide (DMF HPLC, 99.9%), 1-Methyl-2-pyrrolidinone (NMP, 98%), methanol (MeOH, HPLC 99%), methanesulfonic acid (MSA, 99.5%), phosphorus pentoxide powder (P_2O_5, 98%), sodium bicarbonate ($NaHCO_3$) were purchased from Sigma-Aldrich. All reagents were used as received. Eaton's reagent (ER) was prepared mixing MSA with P_2O_5 (10:1 wt/wt) at 30 °C under N_2.[33] The ER was used immediately after being prepared.

Characterization. The characterization of the prepared composite membranes was performed using different equipment's. Nuclear magnetic resonance (^{1}H NMR) spectra were recorded with a Bruker Alpha ATR spectrometer operating at 400 MHz using DMSO-d_6 as solvent. Inherent viscosities (h_{inh}) of 0.5 g/dL polymer solutions in NMP were measured at 30 ± 0.1 °C using an Ubbelohde viscometer. The thermal stability of the polymers was measured by thermogravimetric analysis (TGA) under N_2 atmosphere at a heating rate of 10 °C/min in the temperature range from 25 to 600 °C on a DuPont 2950 Thermogravimetric Analyzer TA Instruments. Molecular weight (Mw) of the polymers were determined using a high pressure size exclusion chromatographer (HPSEC) Waters 717 plus Autosampler, equipped with two columns: Styragel HR 4E molecular weight range from 5×10^2 to 1×10^5 and Styragel HR 5E from 2×10^3 to 4×10^6. DMF was used as an eluent at 50 °C with a flow rate of 1.0 mL/min and linear poly(methyl methacrylate) was used as a standard. The internal microscopic morphologies of different PBI composite membranes were studied by field emission scanning electron microscope (FE–SEM) and the conductivity in the transverse direction was measured by electrochemical impedance spectroscopy (EIS). The measurements were carried out on composite membranes at several temperatures in the range 20–200 °C and a frequency window from 0.1 Hz to 10 MHz. The experiments were performed with 100 mV amplitude, using a Novocontrol broadband dielectric spectrometer (Hundsangen, Germany) integrated by a SR 830 lock-in amplifier with an Alpha dielectric interface. During the measurements, the temperature was maintained isothermally controlled using a nitrogen jet (QUATRO from Novocontrol) with a temperature error of 0.1 °C during every single sweep in frequency.

Synthetic procedures.

Synthesis of PBI–2. The synthesis of PBI–2 was performed using a mixture of OBBA diacid (258 mg, 1.0 mmol) and TAB (214 mg, 1.0 mmol) in a 50 mL Schlenk flask, previously degassed three times using nitrogen-vacuum cycle. Then, the flask was filled with 4.5 mL of freshly prepared Eaton's reagent, which was prepared mixing MSA with P_2O_5 (10:1 wt/wt) at 30 °C under N_2. The mixture was stirred at room temperature for 10 min, until obtaining a homogeneous solution. Next, a $CaCl_2$ tramp with constant N_2 atmosphere was adapted. Finally, the flask was placed into an oil bath preheated at 180 °C, and the reaction was stopped when a viscous solution was obtained. The product was immediately isolated by pouring into $NaHCO_3$ water solution, then it was filtered off and washed around three times with deionized water until obtained the residual water with neutral pH and finally washed with methanol. The polymer was dried in a vacuum oven at 60 °C for approximately 6 h to a constant weight. ^{1}H NMR (400 MHz, DMSO-d_6), d (ppm): 13.01 (s, 1H), 8.31–8.29 (d, 2H), 7.98 (s, 1H), 7.79 (s, 1H), 7.59 (s, 1H) and 7.33–7.31 (d, 2H).

Synthesis of PBI–3. The synthesis of PBI–3 was performed similarly to PBI–2 but using HFA diacid (392 mg, 1.0 mmol) and TAB (214 mg, 1.0 mmol) in 5.5 mL of freshly prepared Eaton's reagent at 180 °C. 1H–NMR (400 MHz, DMSO-d_6), d (ppm): 13.20 (s, 1H), 8.39–8.36 (d, 2H), 8.10 (s, 1H), 7.83 (s, 1H), and 7.64–7.62 (d, 3H).

Synthesis of H[COSANE]. The $H[Co((C_2B_9H_{11})_2]$ named H[COSANE] was obtained from liquid-liquid extraction from the corresponding cesium salt, $Cs[Co((C_2B_9H_{11})_2]$, following a described methodology [32]. To this end, 200 mg of $Cs[Co((C_2B_9H_{11})_2]$ were dissolved in 20 mL of diethyl ether. The sample was transferred to a separatory funnel and 15 mL of 1 M HCl was added. After two phases were formed, the metallacarborane sample was transferred to the organic layer. Next, the organic layer was extracted with 1 M HCl (3 × 15 mL) to completely replace Cs^+ to H^+. Then, a powder of H[COSANE] was obtained after drying in vacuum.

Membrane preparation. The composite polymeric membranes films were fabricated using the casting method. For this, H[COSANE] was dissolved in the PBI–1, PBI–2 or PBI–3 solution, using DMAc as solvent, under stirring to obtain the PBI solution of different of H[COSANE]. Then, the prepared solution was cast onto a glass plate and dried at 80 °C for 8 h, then was dried at 160 °C for 24 h to remove the residual solvent (DMAc). Finally, the composite membranes were peeled off the glass plate and dried under vacuum at 160 °C for 6 h.

Conflicts of interest

There are no conflicts to declare.

Acknowledgements

This work was financially supported by the Ministerio de Economía y Competitividad (MINECO) under project ENE/2015-69203-R and by Consejo Nacional de Ciencia y Tecnologia (CONACyT) for the postdoctoral grant to J. O. The technical support of Servei de Microscòpia Electrònica at Universitat Politècnica de València and Servei Central d'Instrumentació Científica at Universitat Jaume I is gratefully acknowledged. The authors thanks Prof. Santiago V. Luis (from Universitat Jaume I) and Dra. Isabel Fuentes, Prof. Francesc Teixidor and Prof. Clara Viñas (from Instituto de Materiales de Barcelona, CSIC), for technical support in H[COSANE] synthesis.

Notes and references

1 https://earthsky.org/earth/atmospheric-co2-record-high-may-2019.
2 B. C. H. Steele and A. Heinzel, *Nature*, 2001, **414**, 345–352.
3 S. J. C. Cleghorn, X. Ren, T. E. Springer, M. S. Wilson, C. Zawodzinski, T. A. Zawodzinski and S. Gottesfeld, *Int. J. Hydrogen Energy*, 1997, **22**, 1137–1144.
4 Y. Wang, K. S. Chen, J. Mishler, S. C. Cho and X. C. Adroher, *Appl. Energy*, 2011, **88**, 981–1007.
5 J. Savage, Y.-L. S. Tse and G. A. Voth, *J. Phys. Chem. C*, 2004, **118**, 17436–17445.
6 K. A. Mauritz and R. B. Moore, *Chem. Rev.*, 2004, **104**, 4535–4586.
7 A. Kraytsberg and Y. Ein-Eli, *Energy Fuels*, 2004, **28**, 7303–7330.
8 M. A. Hickner, H. Ghassemi, Y. S. Kim, B. R. Einsla and J. E. McGrath, *Chem. Rev.*, 2004, **104**, 4587–4612.
9 O. E. Kongstein, T. Berning, B. Borresen, F. Seland and R. Tunold, *Energy*, 2007, **32**, 418–422.

10 J. Escorihuela, A. García-Bernabé, A. Montero, A. Andrio, O. Sahuquillo, E. Giménez and V. Compañ, *Polymers*, 2019, **11**, 1185.
11 Suryani; Y.-N. Chang, J.-Y. Lai and Y.-L. Liu, *J. Membr. Sci*., 2012, **403–404**, 1–7.
12 J. Escorihuela, R. Narducci, V. Compañ and F. Costantino, *Adv. Mater. Interfaces*, 2019, **6**, 1801146.
13 J. Escorihuela, O. Sahuquillo, A. García-Bernabé, E. Giménez and V. Compañ, *Nanomaterials*, 2018, **8**, 775.
14 I. Fuentes, A. Andrio, A. Garcia-Bernabé, J. Escorihuela, C. Viñas, F. Teixidor and V. Compañ, *Phys. Chem. Chem. Phys*., 2018, **20**, 10173–10184.
15 M. Watanabe, M. L. Thomas, S. Zhang, K. Ueno, T. Yasuda and K. Dokko, *Chem. Rev*., 2017, **117**, 7190–7239.
16 J. Escorihuela, A. García-Bernabé, A. Montero, O. Sahuquillo, E. Giménez and V. Compañ, *Polymers*, 2019, **11**, 732.
17 J. Dechnik, J. Gascon, C .J. Doonan, C. Janiak and C. J. Sumby, *Angew. Chem. Int. Ed*., 2017, **56**, 9292–9310.
18 T.-S. Chung, L. Y. Jiang, Y. Li and S. Kulprathipanja, *Prog. Polym. Sci*., 2007, **32**, 483−507.
19 J. Zhang, Z. Xie, J. Zhang, Y. Tang, C. Song, T. Navessin, Z. Shi, D. Song, H. Wang, D. P. Wilkinson, Z.-S. Liu and S. Holdcroft, *J. Power Sources*, 2006, **160**, 872–891.
20 S. S. Araya, F. Zhou, V. Liso, S. L. Sahlin, J. R. Vang, S. Thomas, X. Gao, C. Jeppesen and S. K. Kaer, *Int. J. Hydrogen Energy*, 2016, **41**, 21310–21344.
21 Y. Cai, Z. Yue and S. Xu, *J. Appl. Polym. Sci*., 2017, DOI: 10.1002/app.44986.
22 J. A. Asensio, E. M. Sánchez and P. Gómez-Romero, *Chem. Soc. Rev*., 2010, **39**, 3210–3239.
23 Y. Wang, Z. Shi, J. Fang, H. Xu and J. Yin, *Carbon*, 2011, **49**, 1199–1207.
24 J. Li, X. Li, Y. Zhao, W. Lu, Z. Shao and B. Yi, *ChemSusChem*, 2012, **5**, 896–900.
25 G. Qian and B. C. Benicewicz, *J. Polym. Sci. Polym. Chem*., 2009, **47**, 4064–4073.
26 X. Li, G. Qian, X. Chen and B. C. Benicewicz, *Fuel Cells*, 2013, **13**, 832–842.
27 R. Nunez, M. Tarres, A. Ferrer-Ugalde, F. F. de Biani and F. Teixidor, *Chem. Rev*., 2016, **116**, 14307–14378.
28 A. Pepiol, F. Teixidor, R. Sillanpää, M. Lupu and C. Viñas, *Angew. Chem. Int. Ed.*, 2011, **50**, 12491–12495.
29 P. González-Cardoso, A. Stoica, P. Farràs, A. Pepiol, C. Viñas and F. Teixidor, *Chem. Eur. J*., 2010, **16**, 6660–6665.
30 M. Tarres, C. Viñas, A. M. Cioran, M. M. Hanninen, R. Sillanpaa and F. Teixidor, *Chem. Eur. J*., 2014, **20**, 15808– 15815.
31 M. Tarrés, V.S. Arderiu, A. Zaulet, C. Viñas, F.F. de Biani and F. Teixidor, *Dalton Trans*., 2015, **44**, 11690-11695.
32 I. Fuentes, A. Andrio, F. Teixidor, C. Viñas and V. Compañ, *Phys. Chem. Chem. Phys*., 2017, **19**, 15177–15186
33 P.E. Eaton, G.R. Carlson and J.T. Lee, *J. Org. Chem*., 1973, **38**, 4071–4073.
34 P. Musto, F.E. Karasz and W.J. Macknight, *Polymer*, 1989, **30**, 1012–1021.
35 H. Xu, K. Chen, X. Guo, J. Fang and J. Yin, *Polymer*, 2007, **48**, 5556–5564.
36 S. Kumar, B. Sana, G. Unnikrishnan, T. Jana and S. Kumar K. S., *Polym. Chem*., 2020, **11**, 1043–1054.
37 S.W. Chuang and S. Hsu, *J. Polym. Sci. A Polym. Chem*., 2006, **44**, 4508–4513.
38 Y. Saegusa, M. Horikiri and S. Nakamura, *Macromol. Chem. Phys*., 1997, **198**, 1619–1625.
39 J.Y. Han, J.Y. Lee, H.-J. Kim, M.-H. Kim, S.G. Han, J.H. Jang, E.A. Cho, S.J. Yoo and D. Henkensmeier, *J. Appl. Polym. Sci*., 2014, **131**, DOI: 10.1002/ app.40521.
40 S.W. Chuang, S.L. Hsu and C.L. Hsu, *J. Power Sources*, 2007, **168**, 172–177.
41 Y. Kang, J. Zou Z. Sun, F. Wang, H. Zhu, K. Han, W. Yang, H. Song and Q. Meng, *Int. J. Hydrogen Energy*, 2013, **38**, 6494–6502.
42 F. Mack, K. Aniol, C. Ellwein, J. Kerres and R. Zeis, *J. Mater. Chem. A*, 2015, **3**, 10864–10874.
43 Y. Kang, J. Zou, Z. Sun, F. Wang, H. Zhu, K. Han, W. Yang, H. Song and Q. Meng, *Int. J. Hydrogen Energy*, 2013, **38**, 6494–6502.
44 D. Ergun, Y. Devrim, N. Bac and I. Eroglu, *J. Appl. Polymer Sci*., 2012, **124**, E267–E277.
45 S. Yuan, G. Yan, Z. Xia, X. Guo, J. Fang and X. Yang, *High Perform. Polym*., 2014, *26*, 212–222.
46 A. Sacco, *Renew. Sust. Energy Rev*., 2017, **79**, 814–829.
47 P.M. Gomadam and J.W. Weidner, *Int. J. Energy Res*., 2005, **29**, 1133–1151.
48 R.J. Klein, S. Zhang S. Dou, B.H. Jones, R.H. Colby and J. Runt, *J. Chem. Phys*., 2006, **124**, 144903.
49 A. Serguei, M. Tress, J. R. Sangoro and F. Kremer, *Phys. Rev. B*., 2009, **80**, 184301.
50 J. Leys, M. Wübbenhorst, C.P. Menon, R. Rajesh, J. Thoen, C. Glorieux, P. Nockemann, B. Thijs, K. Binnemans and S. Longuemart, *J. Chem. Phys*., 2008, **128**, 064509.
51 E.M. Trukhan, *Sov. Phys. Solid State*, 1963, **4**, 2560–2570.
52 R. Coelho, *Rev. Phys. Appl*., 1983, **18**, 137–146.
53 R. Coelho, *J. Non-Cryst. Solids*, 1991, **131–133**, 1136–1139.
54 E. Barsoukov and J.R. MacDonald, Impedance Spectroscopy: Theory, Experiment and applications, Wiley-Interscience, Hoboken, NJ, 2005.
55 D.C. Villa, S. Angioni, S. Dal Barco, P. Mustarelli and E. Quartarone, *Adv. Energy Mater*., 2014, **4**, 1301949.
56 Y.-L. Ma, J.S. Wainright, M.H. Litt and R.F. Savinell, *J. Electrochem. Soc*., 2004, **151**, A8–A16.
57 Q. Li, J.O. Jensen, R.F. Savinell and N.J. Bjerrum, *Prog. Polym. Sci*., 2009, **34**, 449–477.
58 S.R. Kumar, J.-J. Wang, Y.-S. Wu, C.-C. Yang and S.J. Lue, *J. Power Sources*, 2020, **445**, 227293.
59 N. Guerrero-Moreno, D. Gervasio, A. Godínez-García and J.F. Pérez-Robles, *J. Power Sources*, 2015, **300**, 229–237.
60 N. Uregen, K. Pehlivanoglu, Y. Ozdemir and Y. Devrim, *Int. J. Hydrogen Energy*, 2017, **42**, 2636–2647.
61 J. Yang, L. Gao, J. Wang, Y. Xu, C. Liu and R. He, *Macromol. Chem. Phys*., 2017, **218**, 1700009.
62 B.S. Kumar, B. Sana, D. Mathew, G. Unnikrishnan and T. Jana, K.S.S. Kumar, *Polymer*, 2018, **145**, 434–446.
63 S. Singha and T. Jana, *ACS Appl. Mater. Interfaces*, 2014, **6**, 21286−21296.
64 Y. Yamazaki, M. Y. Jang and T. Taniyama, *Adv. Mater*., 2004, **5**, 455−459.
65 R. Kannan, H. N. Kagalwala, H. D. Chaudhari, U.K . Kharul, S. Kurungot and V. K. Pillai, *J. Mater. Chem*., 2011, **21**, 7223–7231.
66 C. Xu, Y. Cao, R. Kumar, X. Wu, X. Wang and K. Scott, *J. Mater. Chem*., 201, **21**, 11359–11364.
67 M. Mamlouka, P. Ocon and K. Scott, *J. Power Sources*, 2014, **245**, 915–926.
68 I. Fuentes, M. J. Mostazo-López, Z. Kelemen, V. Compañ, A. Andrio, E. Morallon, D. Cazorla-Amorós, C. Viñas and F. Teixidor, *Chem. Eur. J*., 2019, **25**, 14308–14319.
69 T. E. Springer, T. A. Zawodzinski and S. Gottesfeld, *J. Electrochem. Soc*., 1991, **138**, 2334–2342.
70 J. Otomo, N. Minagawa, C. Wen, K. Eguchi, H. Takahashi, *Solid State Ionics*, 2003, **156**, 357–369.
71 M. A. Gebbie, A. M. Smith, H. A. Dobbs, A. A. Lee, G. G. Warr, X. Banquy, M. Valtiner, M. W. Rutland, J. N. Israelachvili, S. Perkin and R. Atkin, *Chem. Commun*., 2017, **53**, 1214–1224.
72 H. Weingärtner, *Angew. Chem. Int. Ed*., 2008, **47**, 654–670.
73 A. Rivera and E. A. Rössler, *Phys. Rev. B*, 2006, **73**, 212201.

74 H. Pu, L. Lou, Y. Guan, Z. Chang and D. Wan, *J. Membrane Sci*., 2012, **415–416**, 496–503.
75 T. S. Sorensen and V. Compañ, *J. Chem. Soc., Faraday Trans*., 1995, **91**, 4235–4250.
76 T. S. Sorensen, V. Compañ and R. Diaz-Calleja, *J. Chem. Soc. Faraday Trans*., 1996, **92**, 1947–1957.
77 Y. Wang, F. Fan, A. L. Agapov, T. Sait, J. Yang, X. Yu, K. Hong, J. Mays and A. P. Sokolov, *Polymer*, 2014, **55**, 4067–4076.
78 D. Valverde, A. Garcia-Bernabé, A. Andrio, E. García-Verdugo, S. V. Luis and V. Compañ, *Phys. Chem. Chem. Phys*., 2019, **21**, 17923–17932
79 S. H. Lee and J. C. Rasaiah, *J. Chem. Phys*., 2011, **135**, 124505.
80 T. Liang, Y. K. Shin, Y.-T. Cheng, D. E. Yilmaz, K. G. Vishnu, O. Verners, C. Zou, S. R. Phillpot, S. B. Sinnott and A. C. T. van Duin, *Annu. Rev. Mater. Res*., 2013, **43**, 109–129.
81 Y. Wang, C.-N. Sun, F. Fan, J. R. Sangoro, M. B. Berman, S. G. Greebaum, T. A. Zawodzinski and A. P. Sokolov, *Phys. Rev. E*., 2013, **87**, 042308.

Supplementary Information for

Study on cobalt metallacarborane salt on different polybenzimidazole membranes for high temperature PEMFC applications

Jessica Olvera [a], Jorge Escorihuela [b,], Larissa Alexandrova [a], Andreu Andrio [c], Abel García-Bernabé [d], Luis Felipe del Castillo [a] and Vicente Compañ [d,*]*

[a] Departamento de polímeros, Instituto de Investigaciones en Materiales, Universidad Nacional Autónoma de México (UNAM), Ciudad Universitaria, Apartado Postal 70-360, Coyoacán, Ciudad de México, 04510, México.

[b] Departamento de Química Orgánica, Universitat de València, Av. Vicente Andrés Estellés s/n, Burjassot 46100 Valencia, Spain.

[c] Departament de Física aplicada, Universitat Jaume I, 12080, Castelló, Spain.

[d] Departamento de Termodinámica Aplicada (ETSII), Universitat Politècnica de Valencia, Campus de Vera s/n. 46022 Valencia, Spain.

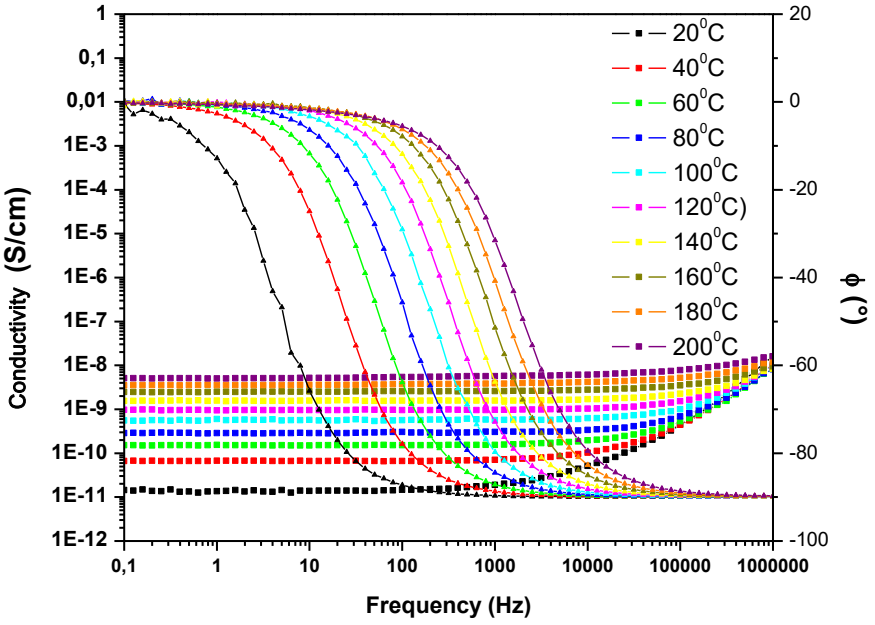

Fig. S1. Bode diagram for the conductivity of undoped composite membrane PBI-1-10%H[COSANE] in the range of temperatures from 20 to 200 ºC.

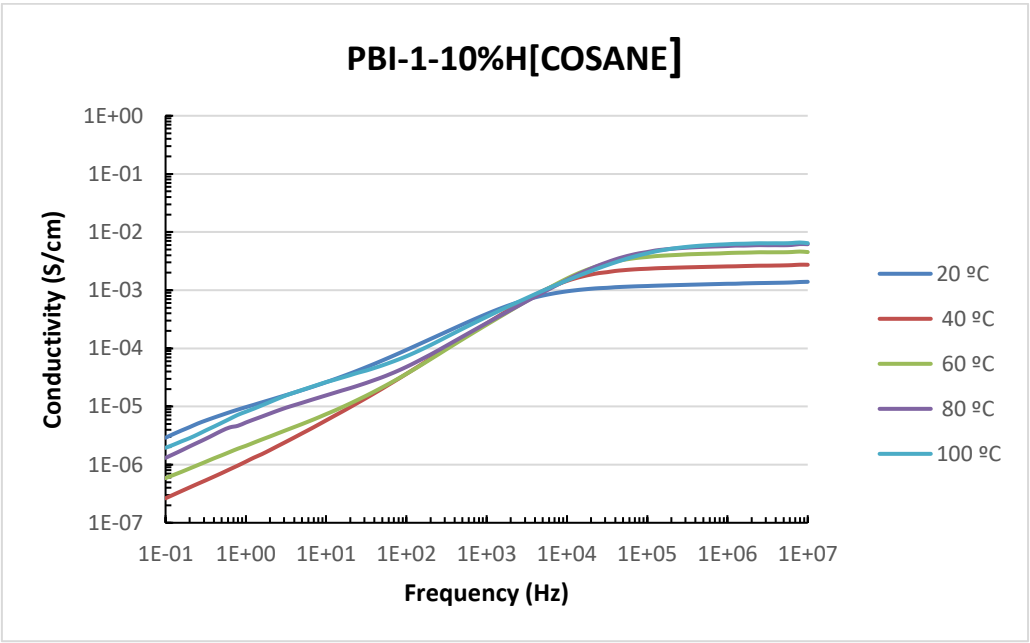

Fig. S2. Conductivity of doped (1 M H_3PO_4) composite membrane PBI-1-10%H[COSANE] in the range of temperatures from 20 to 100 ºC.

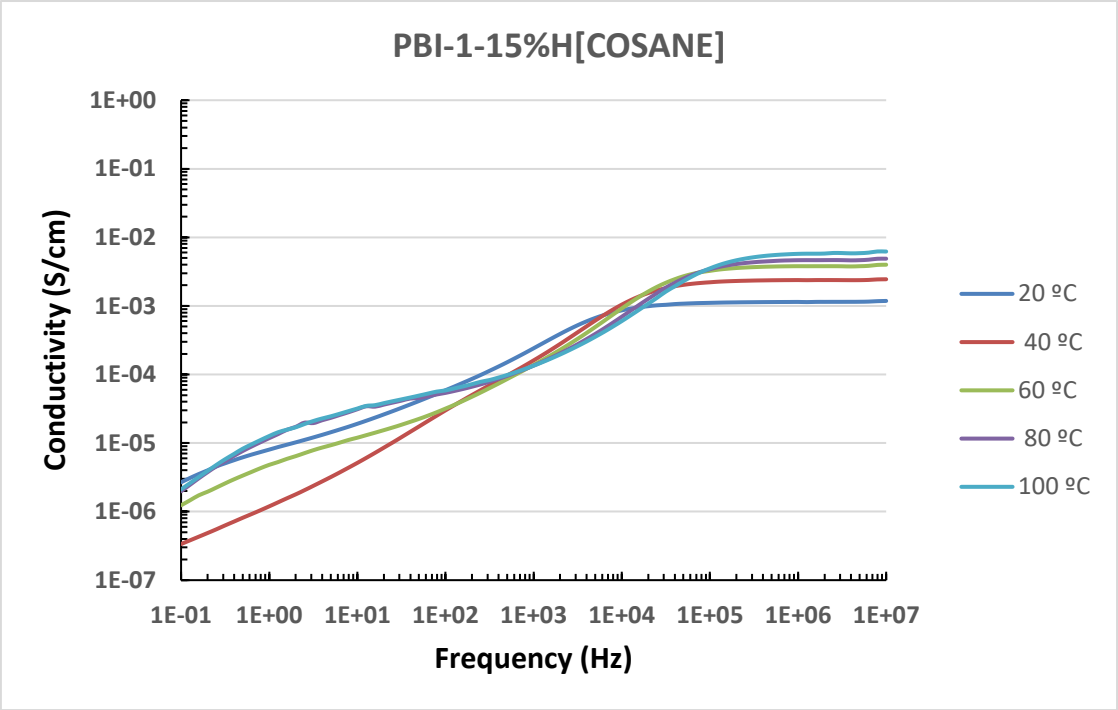

Fig. S3. Conductivity of doped (1 M H_3PO_4) composite membrane PBI-1-15%H[COSANE] in the range of temperatures from 20 to 100 ºC.

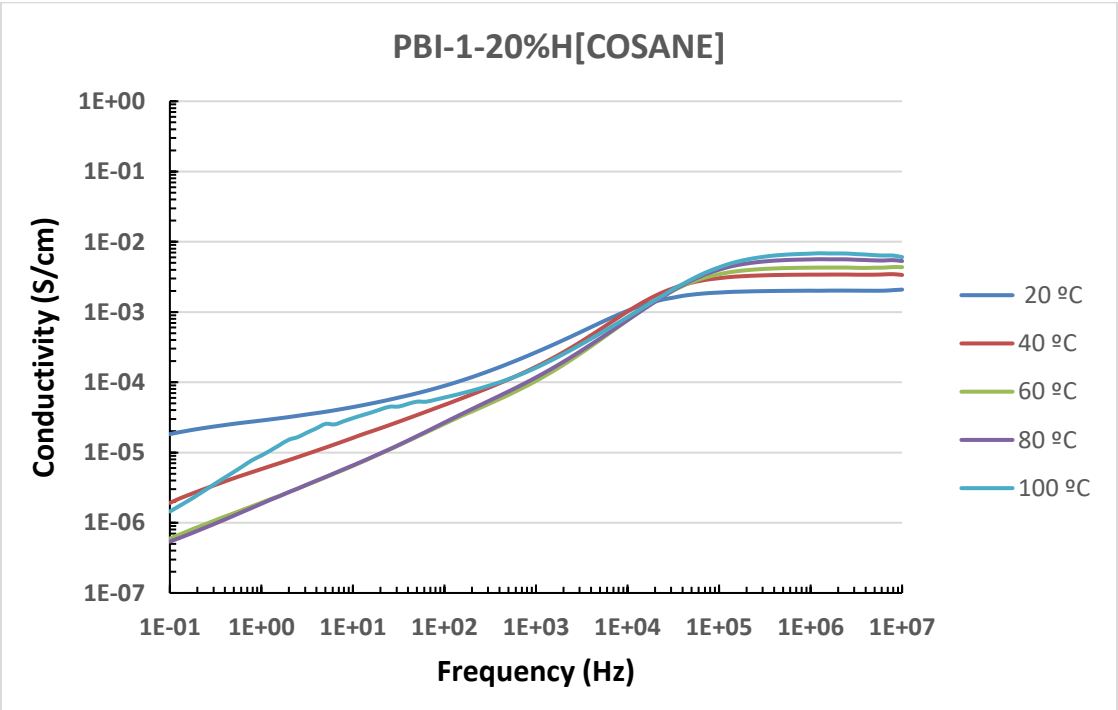

Fig. S4. Conductivity of doped (1 M H_3PO_4) composite membrane PBI-1-20%H[COSANE] in the range of temperatures from 20 to 100 ºC.

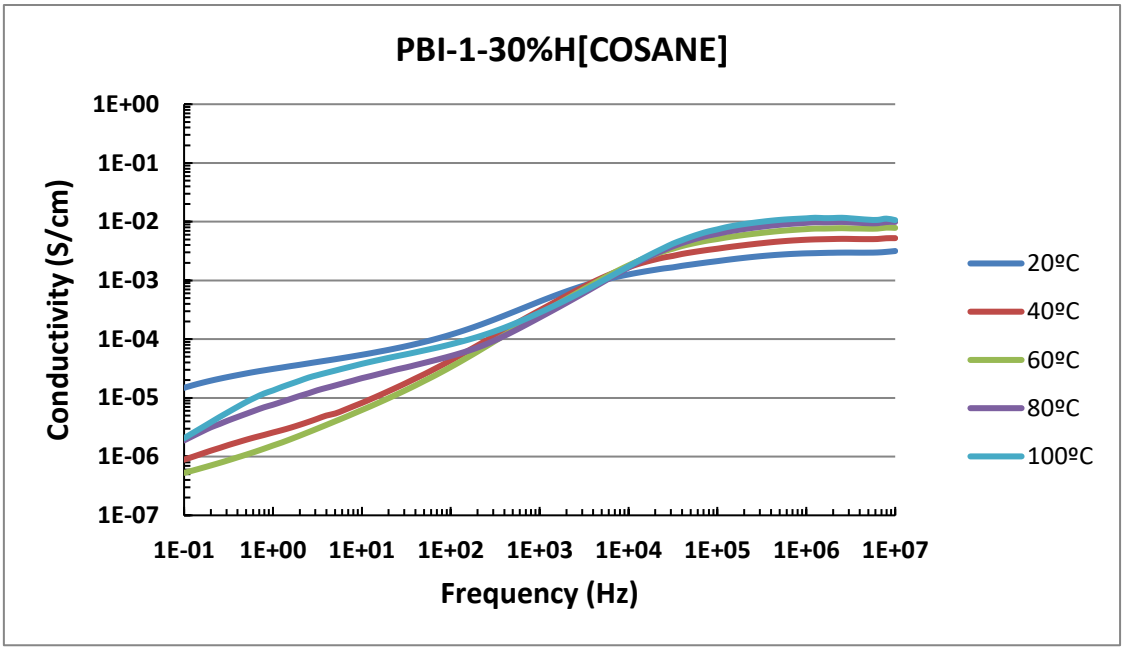

Fig. S5 Conductivity of doped (1 M H_3PO_4) composite membrane PBI-1-30%H[COSANE] in the range of temperatures from 20 to 100 ºC.

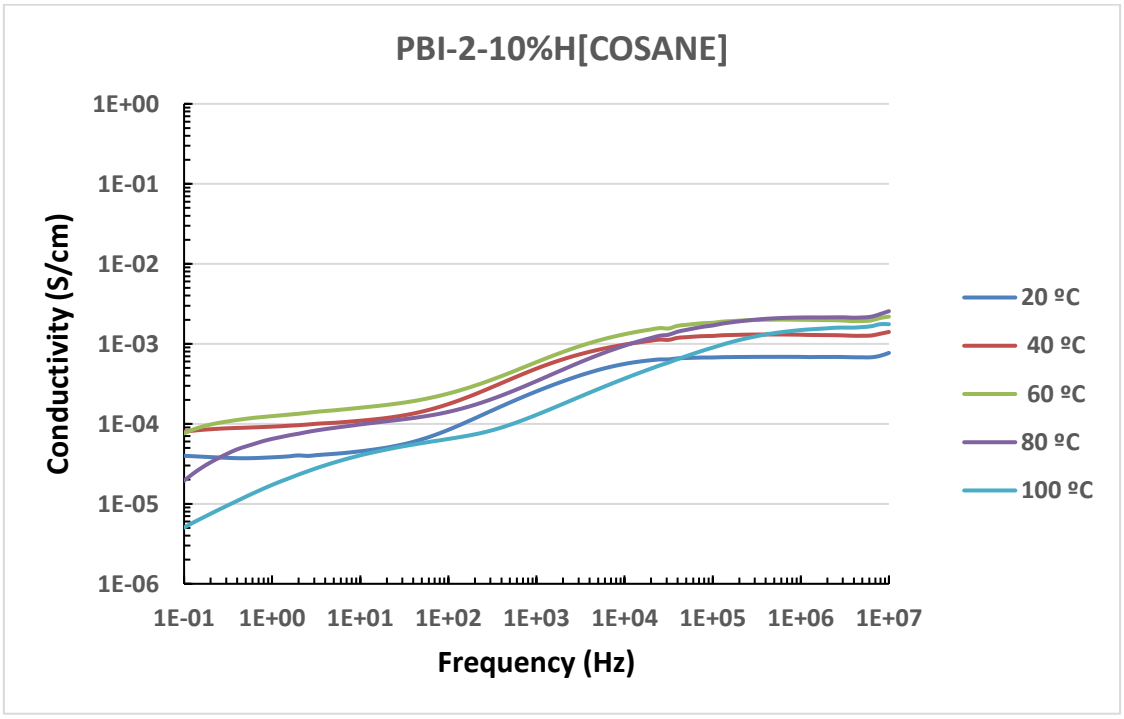

Fig. S6. Conductivity of doped (1 M H_3PO_4) composite membrane PBI-2-10%H[COSANE] in the range of temperatures from 20 to 100 ºC.

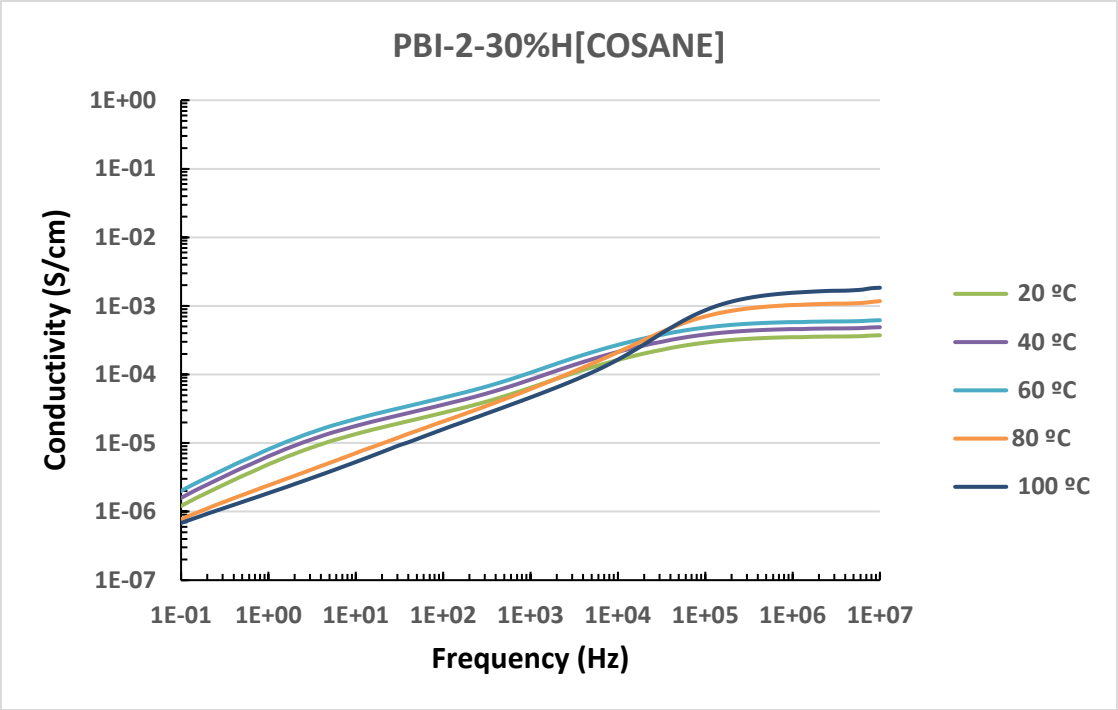

Fig. S7. Conductivity of doped (1 M H_3PO_4) composite membrane PBI-2-30%H[COSANE] in the range of temperatures from 20 to 100 ºC.

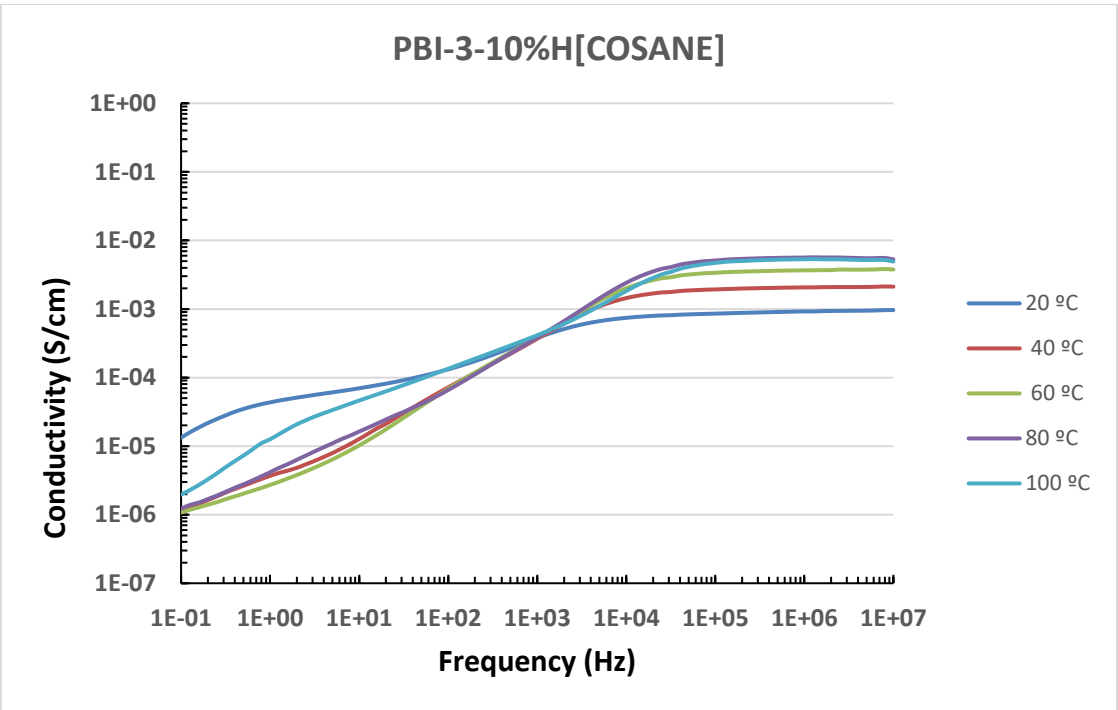

Fig. S8. Conductivity of doped (1 M H_3PO_4) composite membrane PBI-3-10%H[COSANE] in the range of temperatures from 20 to 100 ºC.

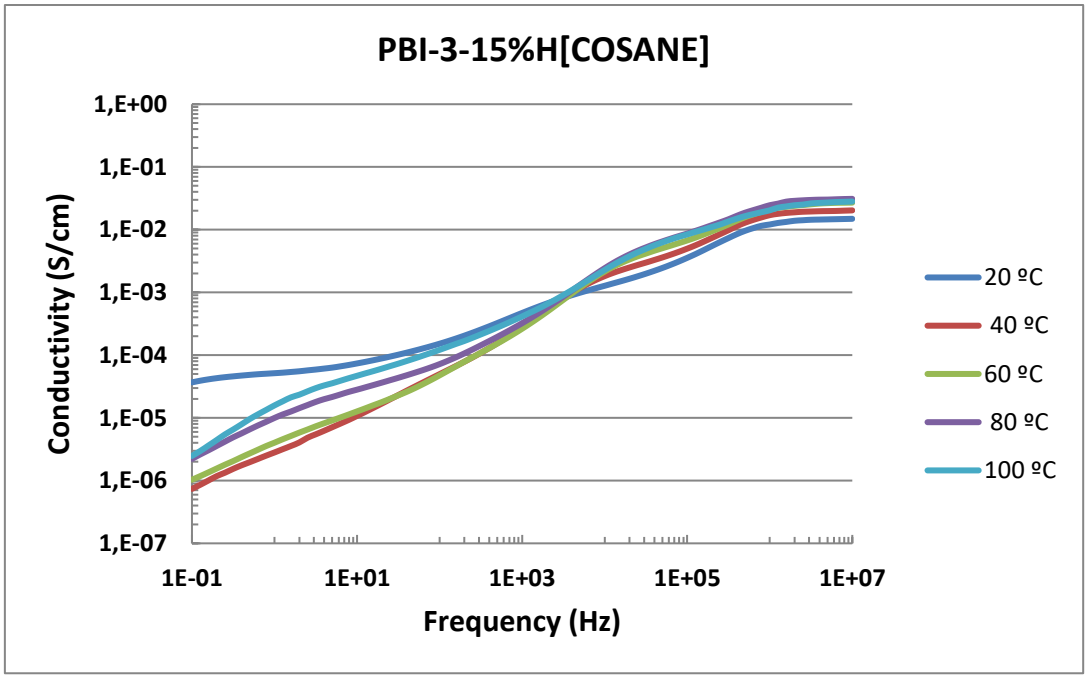

Fig. S9. Conductivity of doped (1 M H_3PO_4) composite membrane PBI-3-15%H[COSANE] in the range of temperatures from 20 to 100 ºC.

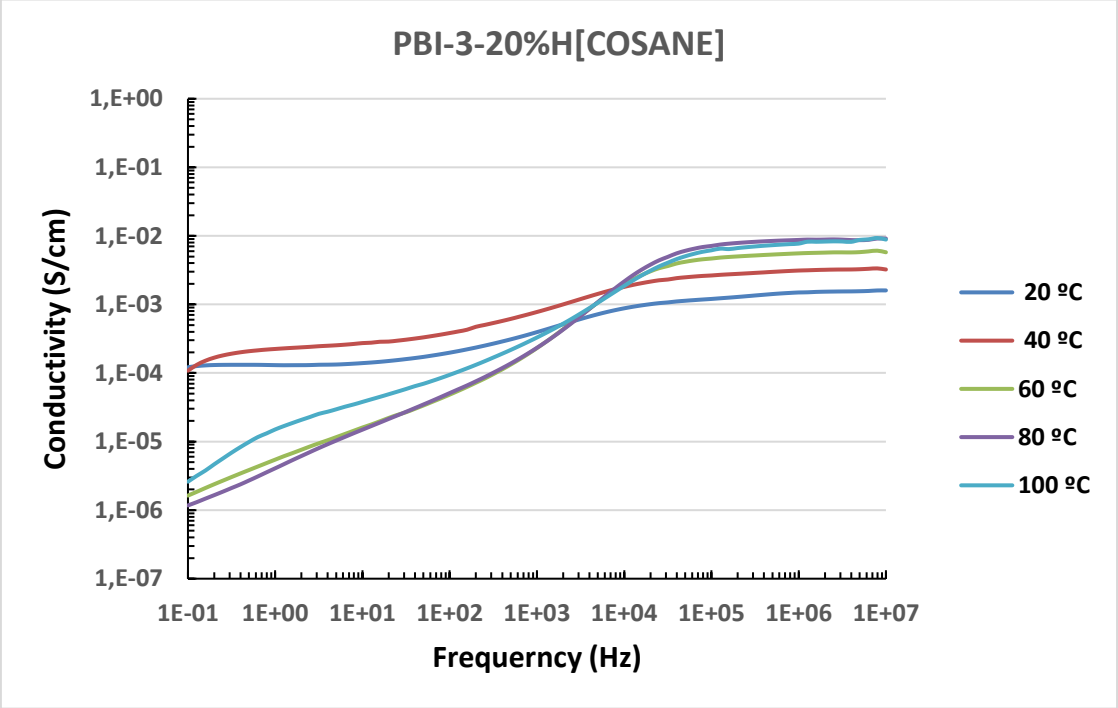

Fig. S10. Conductivity of doped (1 M H_3PO_4) composite membrane PBI-3-20%H[COSANE] in the range of temperatures from 20 to 100 ºC.

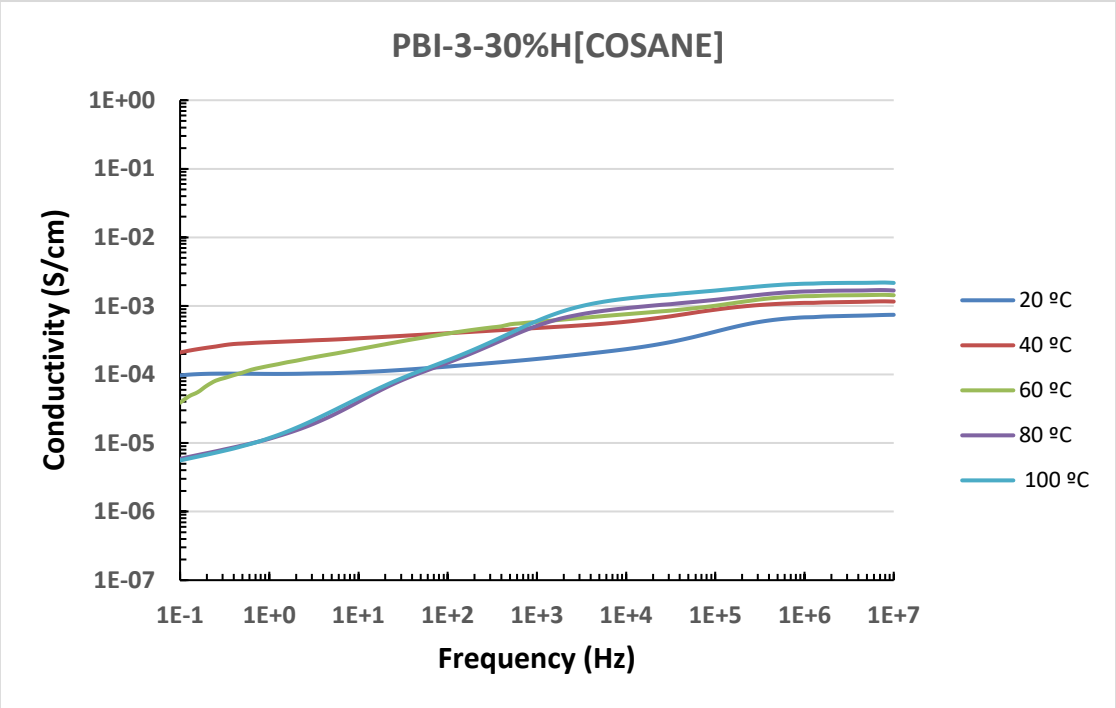

Fig. S11. Conductivity of doped (1 M H_3PO_4) composite membrane PBI-3-30%H[COSANE] in the range of temperatures from 20 to 100 ºC.